PAPER

Check for updates

Olefin metathesis in confined spaces: the encapsulation of Hoveyda–Grubbs catalyst in peanut, square, and capsule shaped hollow silica gels†

Mina Aşkun,[a] Kutay Sagdic, [iD][bc] Fatih Inci [iD][bc] and Bengi Özgün Öztürk [iD]*[a]

In this study, Hoveyda–Grubbs 2nd generation (HG2) catalyst was encapsulated in hollow mesoporous silica gels with various morphologies (peanut, square, and capsule) by reducing the pore size of the mesoporous shell. The resulting catalytic system efficiently catalyzed the ring-closing metathesis of diethyl diallylmalonate, as well as the ethenolysis reactions of methyl oleate and fatty acid methyl ester mixtures. The interior void in hollow silica gel provided a confined isolated site for both ruthenium catalyst and olefinic substrates where the performance and recyclability in metathesis reactions were improved compared to the homogenous analogs. Finally, the catalyst could be easily recycled and used in ring-closing metathesis of diethyl diallylmalonate up to the 10th turn. In sum, this study has demonstrated that hollow silica gels are efficient materials for the encapsulation of homogenous catalysts, which improve the stability of the HG2 even under an air atmosphere, maintaining its activity for up to 6 months of storage time on the benchtop.

Introduction

Olefin metathesis is an efficient tool to construct complex molecular structures with carbon–carbon double bonds.[1] Metathesis chemistry has garnered notable attention with the invention of moisture and functional group tolerant ruthenium-based Grubbs and Hoveyda–Grubbs type catalysts.[2] Following the development of different variants of Grubbs and Hoveyda–Grubbs type catalysts, olefin metathesis became a vital tool to build both synthetic and natural products that are not accessible to the other well-known synthetic methods.[3] Although Hoveyda–Grubbs type catalysts are employed in various olefin metathesis and non-metathetic organic transformation reactions, the reusability and the separation of these ruthenium-based homogenous catalysts is an ongoing challenge.[4] Immobilizing metathesis catalysts onto various polymeric or inorganic support materials through covalent or ionic bonds addresses the challenges faced in the separation and reusability; yet, this immobilization strategy requires the

modification of the catalyst or the support surface.[5,6] Moreover, the activity of the supported catalysts is limited contrary to their homogenous analogs, and in some cases, the diffusion limitations of the substrates to the catalyst surface and the steric environment of the active sites hinder the performance of the catalytic system.[7] As an alternative strategy, water-soluble or amphiphilic polymer-supported ruthenium catalysts have been developed for olefin metathesis reactions in aqueous media where the catalyst can be easily recycled in the aqueous phase; however, both performance and recyclability of the catalyst face significant obstacles in aqueous media due to the ruthenium leaching and catalyst decomposition.[8] Encapsulation of homogenous catalysts within porous materials is an emergent methodology to fulfill the need in the gap between homogenous and heterogeneous catalysts where the immobilization limitations were eliminated. Various homogenous catalysts and nano-sized catalysts were encapsulated in various support materials such as metal–organic frameworks, silica gels, biopolymers, porous polymers, and self-assembled molecules/polymers.[9] For instance, a straightforward strategy was established to encapsulate various transition metal complexes in nanocages of mesoporous silica supports *via* post-pore size reduction procedure where the organosilica groups were utilized to reduce the pore sizes of the support materials.[10] In an earlier example, Hoveyda–Grubbs 2nd generation catalyst was encapsulated within the nanocages of SBA-1 support materials through end-capping the

[a] *Hacettepe University, Faculty of Science, Chemistry Department, Beytepe, Ankara, 06800, Turkey. E-mail: bengi04@hacettepe.edu.tr*
[b] *UNAM—National Nanotechnology Research Center, Bilkent University, 06800 Ankara, Turkey*
[c] *Institute of Materials Science and Nanotechnology, Bilkent University, 06800, Ankara, Turkey*
† Electronic supplementary information (ESI) available. See DOI: https://doi.org/10.1039/d2cy01291j

6174 | *Catal. Sci. Technol.*, 2022, **12**, 6174–6183

This journal is © The Royal Society of Chemistry 2022

pore entrances with bulky diphenyl silane groups.[11] Later on, the same strategy was employed using a yolk–shell structured mesoporous silica to encapsulate HG2 catalyst where the catalyst could be recycled up to the 8th turn without any significant ruthenium leaching.[12] Recently, our research group employed a hydrophobic core/hydrophilic shell approach to encapsulate HG2 in mesoporous carbon/alginate gels to conduct olefin metathesis in aqueous media.[13] While compared with the other inorganic support materials, hollow silica gels have superior fashions such as high specific surface area, low density, and high encapsulation efficiency owing to the extensive void volume within the silica structure.[14] The physical assets and morphology of hollow silica gels can be controlled easily through soft or hard template-based synthesis methods.[15] In addition, hollow silica gel with peanut, square, and capsule-shaped morphologies are accessible through Stöber methods utilizing iron(III) oxides as hard-templates. Up to date, metal nanoparticles and enzymes were encapsulated in hollow silica gels which are high-yielded, efficient, and reusable catalysts for various organic transformation reactions.[15–17] The high adsorption capacity, low density, and high void space of hollow silica gels make them ideal support materials for the catalyst encapsulation process.

Herein, we have encapsulated Hoveyda–Grubbs 2nd generation catalyst in peanut, square, and capsule-shaped hollow silica gels through post-pore size reduction. Comparing to the homogenous counterparts, the performance of the catalyst is improved in the means of recyclability and performance in ring-closing metathesis and ethenolysis reactions. Moreover, the catalyst can be easily recycled and can be used up to 10 times without any significant ruthenium leaching.

Results and discussion

The encapsulation of homogenous catalysts in confined spaces is an interesting concept owing to the uniqueness of the catalytic systems harmonizing the advantages of homogenous and heterogeneous catalysts.[17] The hollow silica gels synthesized by hard templates offer high void space, low density, and morphology control.[18] In this study, we have used peanut, square, and capsule-shaped hematite (α-Fe₂O₃) as hard templates, followed by coating the hematite particles with SiO₂ using the Stöber method. For this purpose, peanut-shaped iron(III) oxide particles were dispersed in an ethanol/water mixture in the presence of dodecyltrimethyl ammonium bromide (CTAB), and Synperonic®F108 and tetraethoxysilane were added to the basic medium (Scheme 1). CTAB used to form mesoporous channels as the templating agent, and non-ionic surfactant Synperonic®F108 used to prevent the colloidal precipitation of silica gel particles during the coating procedure. Herein, the coated particles were denoted as Fe₂O₃@peanut according to their shapes and characterized by SEM-EDX analysis. The hollow silica gels (peanut, square, and capsule) were synthesized by etching the hard-templating agent (iron(III) oxide) using 6 M HCl under reflux. The samples were washed several times with water and dried at 300 °C overnight.
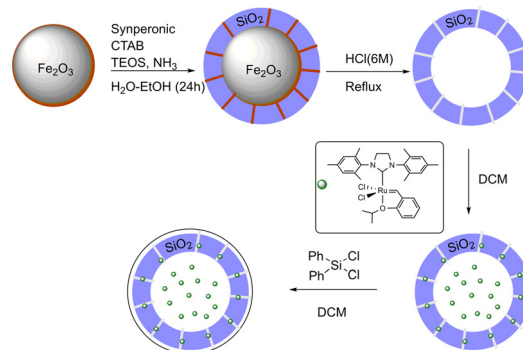
Scheme 1 Encapsulation of HG2 in hollow silica gels.

The hematite particles (peanut, square, and capsule-shaped), silica coated particles (Fe₂O₃@peanut, Fe₂O₃@square, and Fe₂O₃@capsule), and hollow silica gels were characterized by SEM-EDX analysis and SEM images were given in Fig. 1. Both SEM and TEM images confirmed the presence of hollow particles and the removal of the templating agent (Fe₂O₃) (Fig. 1 and 2). The hard template was successfully removed from the core of the silica gel structure As confirmed by TEM, SEM, and EDX analysis (please see ESI,† Fig. S1–S9). The structural integrity of the silica gels was protected during the etching process. The lengths of the particle were 1375 ± 110 nm, 430 ± 65 nm, and 975 ± 145 nm for peanut, square, and capsule-shaped hollow silica gel particles, respectively. We further evaluated the width and thickness of these particles as depicted in Fig. S2–S10.†

Hoveyda–Grubbs 2nd generation catalyst (HG2) was loaded on peanut/square/capsule-shaped hollow silica gels in dichloromethane at room temperature under a nitrogen atmosphere (Scheme 1) for 24 h. After that, the pore-size reducing agent (dichlorodiphenylsilane), was added to the reaction media followed by the addition of 2-methylpyridine. The reaction mixture was stirred for 12 h at room
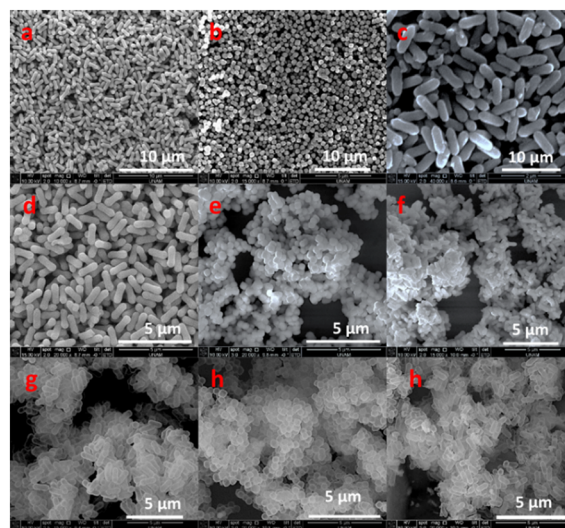
Fig. 1 SEM images of Fe₂O₃ (a-peanut, b-square, and c-capsule), SiO₂@Fe₂O₃ (d-peanut, e-square, and f-capsule), and hollow silica gels (g-peanut, h-square, and h-capsule).

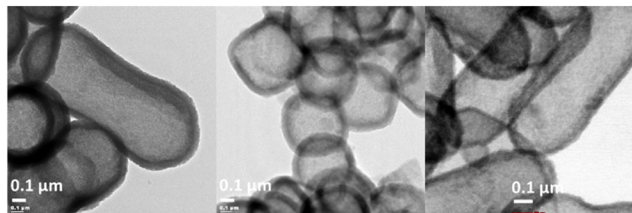**Fig. 2** High contrast TEM images of hollow peanut, square, and capsule silica gels.

Table 1 Surface properties of hollow silica gels

	Surface area[a] ($m^2 \, g^{-1}$)	Pore volume ($cm^3 \, g^{-1}$)	Pore size[b] (nm)
Hollow peanut	380	1.94	7.1
HG2@peanut	245	0.64	5.1
en-HG2@peanut	183	0.26	4.7
Hollow square	780	2.67	15.6
HG-2@square	285	0.93	11.4
en-HG2@square	190	0.22	9.2
Hollow capsule	460	2.03	7.4
HG2@capsule	102	0.72	5.6
en-HG2@capsule	52	0.29	4.6

[a] Determined by N_2 adsorption/desorption isotherms (BET). [b] Average pore size.

temperature and the dichloromethane was removed by vacuum. The resulting green solid was washed several times with toluene to remove unreacted dichlorodiphenylsilane and 2-methylpyridine. UV-vis analysis showed that HG2 catalyst was successfully loaded on silica gel as confirmed by the characteristic π–π* transition peak at 378–380 nm (Fig. 3). The non-encapsulated silica gels were denoted as HG2@peanut, HG2@square, and HG2@capsule, whereas encapsulated analogs were denoted as en-HG2@peanut, en-HG2@square, and en-HG2@capsule.

The surface areas, pore sizes, and pore volumes of hollow silica gels (peanut, square, and capsule), HG2@SiO$_2$, and en-HG2@SiO$_2$ were determined using N$_2$ adsorption/desorption isotherms (Table 1) (ESI,† Fig. S10–S13). Hollow peanut-shaped silica gel had a surface area of 380 m^2 g^{-1} with a pore volume of 1.94 cm^3 g^{-1} and pore size of 7.1 nm. The surface area of the silica gel decreased to 245 m^2 g^{-1} following the addition of HG2 catalyst (HG2@peanut) and the pore volume and size decreased to 0.64 cm^3 g^{-1} and 5.1 nm. After treating the silica gel with the post-pore size reducing agent (dichlorodiphenylsilane), the surface area was decreased to 183 m^2 g^{-1} and the pore volume and size decreased to 0.26 cm^3 g^{-1} and 4.7 nm. Similar results were obtained from the square and capsule-shaped silica gels. The N$_2$ adsorption/desorption analysis showed a type-IV isotherm with a hysteresis loop of type H3, indicating the presence of slit-like pores.[19a]

The molecular size of HG2 was estimated to be 1.76 nm × 1. 35 nm × 1.05 nm as reported by Yang et al.[19b] HG2@peanut has an average pore size of 5.1 nm and the majority of the pores have sizes of 5.45 nm and 2.68 nm. In addition, the mesopores with relatively higher sizes (>5 nm) are also present. Following the silylation procedure, the sizes of these
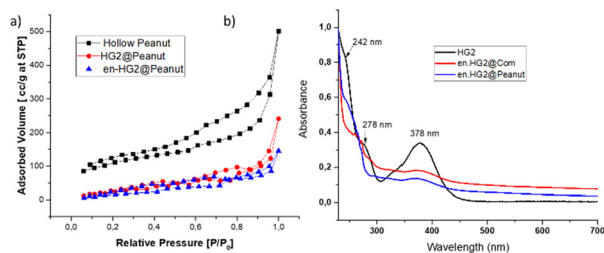
pores decreased to 4.12 nm and 2.13 nm. Although the final pore size was still higher than the dimensions of HG2, ruthenium complex tend to stay in hollow void due to the reduction in pore size, slowing down the outer diffusion of catalyst combined by the steric effect that were exerted by diphenylsilane groups at the outer shell.

The high-contrast TEM images of encapsulated catalysts (en-HG2@peanut, en-HG2@square, and en-HG2@capsule) were exhibited in Fig. 4–6. As shown in HR-TEM and line-scan analysis, the HG2 catalyst was located inside of the hollow spaces of the silica gel (ESI,† Fig. S14–S16). As previously stated, UV-vis and ICP-MS analysis showed that the loading efficiency of the catalyst is 90% wt. Ru 3d$_{5/2}$ signal was not observed at 280–282 eV interval indicating that ruthenium is not located on the outer surface of the catalyst since XPS has only 10 nm penetration range (ESI,† Fig. S17–S19). On the other hand, the presence of ruthenium was confirmed by EDX analysis which has a higher penetration effect (ESI,† Fig. S20–S22).

Fig. 3 a) N$_2$ adsorption/desorption isotherms of hollow peanut, HG2@peanut and en-HG2@peanut; b) UV-vis spectrum of HG2, en-HG2@Com., and en-HG2@peanut in dichloromethane.
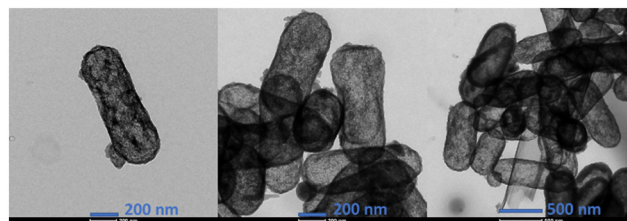

Fig. 4 High contrast TEM images of en-HG2@peanut.
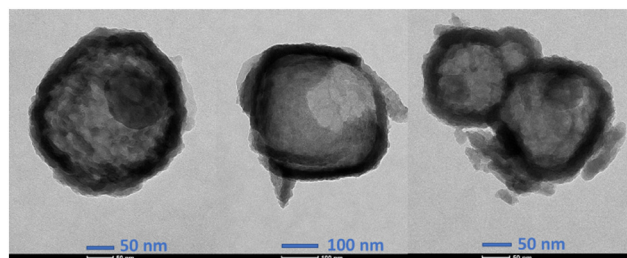
Fig. 5 High contrast TEM images of en-HG2@square.
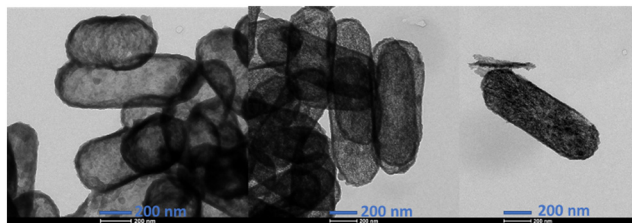
Fig. 6 High contrast TEM images of en-HG2@capsule.

Chart 1 The comparison of catalyst activities on RCM of diethyl diallylmalonate.

Hollow spaces were filled with HG2 and the major part of the catalyst particles were confined in hollow spaces as confirmed by high contrast TEM analysis (Fig. 4–6). It is important to note that after HG2 encapsulation to peanut-shaped silica gel, the neck of the silica gel was expanded and the peanut morphology was transformed into a different shape between peanut and capsule geometry. The same protocol was applied to hollow square silica gels to form en-HG2@square. The expansion of the morphology was also observed in square-shaped silica gels due to the loading of the HG2 in the hollow cavity (Fig. 5).

The performance of the catalysts was first examined with ring-closing metathesis (RCM) reactions of diethyl diallylmalonate (DEDAM) in various organic solvents and aqueous medium and the results were listed in Table 2. Regardless of the silica gel morphology, all catalytic systems showed excellent performance in RCM of DEDAM, reaching quantitive yields in CH_2Cl_2, toluene, and water. The performance of the catalysts was decreased drastically in THF, which is a polar and coordinating solvent that states the deactivation of the catalyst. The effect of post-pore size reduction on the performance of the catalyst was tested on RCM reactions of diethyl diallylmalonate under optimized reaction conditions with a catalytic loading of 1 mol% Ru in CH_2Cl_2 (Chart 1). As can be seen in the kinetic plot of RCM reactions, the reaction proceeded relatively faster in non-encapsulated catalysts regardless of the shape of the support material. The reaction proceeded relatively slower in encapsulated catalyst due to the diffusion limitations exerted by the sterically bulky phenyl groups that are located on the silica surface. The surface area had a slight boosting effect
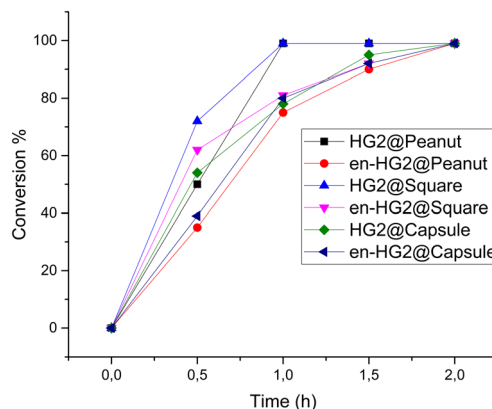
on the RCM performance of the catalyst due to the improved diffusion of substrates to the active sites.

On the next trial, the performance of the encapsulated catalysts was tested on ethenolysis reactions of methyl oleate, a renewable substrate obtained from vegetable oils.[20] Ethenolysis is an efficient cross-metathesis reaction to synthesize terminal olefins from internal olefins in an efficient manner. Ethylene as a sterically unhindered simple olefinic substrate is used for the scission of unsaturated long-chain hydrocarbons as well as unsaturated cyclic molecules.[21] The ethenolysis of methyl oleate was carried out at atmospheric pressure (1 atm) in toluene at 80 °C with a catalytic loading of 1 mol% Ru (en-HG2@peanut) (Table 3). The reaction proceeded smoothly in all cases and the ethenolysis reaction proceeded with high selectivity toward ethenolysis products. Only minor amounts of cross-metathesis products were observed. The cross-metathesis product 9-octadecene was formed in minor amounts and other diester based cross-metathesis product (CM1) was not observed. These results indicate that the cross-metathesis takes place after the formation of the ethenolysis product; 1-decene (E2) which undergoes cross(self)-metathesis to form the corresponding metathesis product (CM2). en-HG2@square showed high performance in ethenolysis of methyl oleate reaching a conversion value of 98% after 1 h of reaction time. The reaction exhibited high selectivity (up to 94%) towards the formation of the ethenolysis product. All catalysts showed similar performance and selectivity in ethenolysis reactions under identical reaction conditions. Hollow silica gel encapsulated HG2 showed improved performance when compared to the performance of the encapsulated HG2 in commercial silica gel.
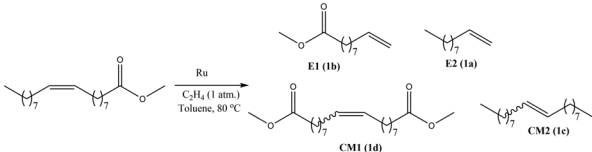
Once the optimum reaction conditions for ethenolysis of methyl oleate were determined using methyl, fatty acid methyl esters obtained from corn oil, rapeseed oil, and waste grounded coffee extract were used as ethenolysis substrates. The fatty acid content of each mixture was given in Table 4. Rapeseed oil has the highest oleic acid content while corn oil is rich in polyunsaturated acid (linoleic acid). Fatty acid

Table 2 RCM reactions catalyzed by encapsulated HG2 catalysts

		Conversion[a] %			
Solvent	Time (h)	Peanut	Square	Capsule	Ru leaching[b] %
CH_2Cl_2	2	99	99	99	—
Toluene	2	99	99	99	—
THF	12	15	12	13	—
Water	2	95	94	95	—

[a] Determined by GC-MS using *n*-tetradecane as the internal standard.
[b] Determined by ICP-MS and UV-vis analysis.

This journal is © The Royal Society of Chemistry 2022

Catal. Sci. Technol., 2022, **12**, 6174–6183 | **6177**

Table 3 Ethenolysis of methyl oleate using encapsulated catalysts

Catalyst	Ru[a] %	Conv.[b] %	Time (h)	Yield[c] %			
				E1	E2	CM1	CM2
en-HG2@capsule	1	95	1	90	90	—	5
	0.5	72	1.5	71	71	—	1
HG2@capsule	1	89	0.5	88	88	—	—
en-HG2@Peanut	1	93	1	91	91	—	2
	0.5	70	1.5	70	70	—	—
HG2@Peanut	1	90	1	90	90	—	—
en-HG2@square	1	98	1	94	94	—	4
	0.5	76	1.5	74	74	—	2
HG2@square	1	91	1	91	91	—	—
en-HG2@Comm.[d]	1	89	4	83	83	—	6
HG2	1	98[e]	1.5	92	92	—	—
G1[f]	1	45	3	45	45	—	—

[a] Please see the Experimental section for detailed information on reaction conditions. [b] Determined by GC-MS using *n*-tetradecane as internal standard. [c] GC yield. [d] Commercial silica gel. [e] Trace amounts of olefin isomerization by-products were observed which decreases the selectivity of the reaction. [f] Grubbs first generation catalyst.

methyl esters obtained from waste coffee extract contain 34% of linoleic and 11% of oleic acid (mole percentage). The fatty acid methyl esters (FAME) were obtained through transesterification of corn and rapeseed (canola) oil with methanol in the presence of sulfuric acid.[22] The grounded coffee extract was obtained following the protocols that were reported in the literature.[23] Fatty acid methyl ester mixtures selectively underwent ethenolysis reactions in the presence of different metathesis catalysts using high-pressure ethylene gas to suppress the undesired self-metathesis reactions.[24] To extend the applicability of the ethenolysis reactions, we have tried to conduct the ethenolysis reactions under atmospheric pressure using standard Schlenk reactors.

The major unsaturated fatty acid methyl esters in both oils are methyl oleate (C18:1) and methyl linoleate (C18:2) which undergo ethenolysis and cross-metathesis reactions in the presence of a metathesis catalyst. The most-common ethenolysis and cross-metathesis products were summarized in Table 5. The reaction reached quantitative yields within 3 h of reaction time in the case of canola and corn oil FAME mixtures using different encapsulated catalysts. The reaction

showed high selectivity towards the formation of ethenolysis products methyl-9-decenoate (E1) and 1-decene (E2) in all cases. It is important to note that the formation of olefin isomerization products is significantly suppressed using encapsulated catalysts when compared to the HG2 catalyzed ethenolysis reactions of FAME mixtures (Table 5, entry 10) which yielded up to 9% isomerization product. The encapsulation of HG2 in hollow peanut, square, and capsule-shaped silica gels, followed by post-pore size reduction process improved the selectivity of the catalyst in the ethenolysis of FAME mixtures as can be seen directly in Table 5. It is interesting to note that ethenolysis products (E4 and E5) of methyl linoleate were observed in case of HG2 catalyzed FAME ethenolysis reactions. The selectivity difference between HG2 and en-HG2@peanut can be explained by the presence of excess ethylene gas that were confined within hollow voids of silica gels which triggers the secondary ethenolysis of E4 and E5 in case of encapsulated catalysts.

Once the catalytic performance of the catalyst was evaluated with RCM and ethenolysis reactions, the reusability

Table 4 Percentage composition of fatty acid methyl ester (FAME) mixtures obtained from different sources

Percentage composition from GC-MS[a]					
	C16	C18			Other fatty acids
	C16:0 (palmitic acid)	C18:1 (oleic acid)	C18:2 (linoleic acid)	C18:0 (stearic acid)	
Corn oil	11	30	51	2	6
Rapeseed oil	8	62	25	3	2
Grounded waste coffee extract (arabica)	43	11	34	8	8

[a] Determined by GC-MS and the percentage values were given as mol fractions.

6178 | *Catal. Sci. Technol.*, 2022, **12**, 6174–6183

This journal is © The Royal Society of Chemistry 2022

Table 5 Ethenolysis of FAME mixtures with different encapsulated catalysts

Entry	Catalyst	FAME	Conversion[a] %	Time	Yield[b,c] %			
					E1	E2	CM1	CM2
1	en-HG2@capsule	Corn	99	3	98	98	—	—
2		Rapeseed	99	3	99	99	—	—
3		Coffee	94	3	94	94	—	—
4	en-HG2@peanut	Corn	99	3	97	97	—	2
5		Rapeseed	99	3	98	98	—	1
6		Coffee	96	3	96	96	—	—
7	en-HG2@square	Corn	99	3	98	98	—	—
8		Rapeseed	99	3	96	96	—	3
9		Coffee	95	3	94	94	—	1
10	HG2	Corn	99	1	91[d]	91	—	—
11		Rapeseed	99	1	90[d]	90	—	—
12		Coffee	98	1	90[d]	90	—	—

[a] Determined by GC-MS using *n*-tetradecane as internal standard. Overall conversion was calculated based on the amounts of methyl oleate and metyl linoleate. [b] GC yield. [c] E3, E4 and E5 were not observed in GC analysis. [d] The trace amounts of E4 and E5 were observed in GC analysis.

of the catalyst systems was tested on RCM of diethyl diallylmalonate using en-HG2@peanut as the representative catalyst. The RCM reaction was carried out with a catalytic loading of 2.5% mol in dichloromethane at 25 °C under a nitrogen atmosphere. The samples that are regularly withdrawn from the reaction mixture were analyzed by GC-MS. Once the conversion of diethyl diallylmalonate reached a plateau, the reaction was centrifuged, and the organic layer was separated. The solid catalyst was washed with dichloromethane, taken to a Schlenk reactor, and used in the next catalytic cycle. The reaction showed high performance until the 6th cycle reaching a conversion value between 80–99% within 1 h of reaction time. After the 6th run, the performance of the catalyst was slightly decreased and the reaction yielded the corresponding RCM product within 2 h of reaction time. After the 10th run, the ruthenium leaching was found to be only 2 wt% which was confirmed by ICP-MS analysis, and hence, the decline in the performance of the

catalyst was due to the decomposition of the catalyst. The long-term stability of the catalyst; en-HG2@peanut, was assessed with RCM reactions of diethyl diallylmalonate. In this regard, en-HG2@peanut catalysts (in solid-state) were stored under an air atmosphere in a closed-glass vial. The activity of the catalyst was tested on RCM of diethyl diallylmalonate regularly within one-month intervals. No significant performance loss was observed in RCM reactions of diethyl diallylmalonate within 6 months of storage time (ESI,† Fig. S23) Table 6.

The high-contrast TEM images of en-HG2@peanut which was isolated after the 6th run in RCM reactions, were recorded and given in Fig. 7. Silica particles were partially ruptured due to the mechanical factors (stirring, centrifugation, swelling/shrinking) during metathesis reaction cycles. However, only a small portion of the silica gels were ruptured and major part of the silica gels maintained their structural integrity. We believe that the

Table 6 Reusability of the en-HG2@peanut catalyst in RCM of diethyldiallyl malonate

Cycle	1	2	3	4	5	6	7	8	9	10[b]
Conversion (%)[a]	99	90	90	90	85	80	70	60	56	52
Time (h)	1	1	1	1	1	1	2	2	4	4

[a] Determined by GC-MS using *n*-tetradecane as internal standard. [b] After the final run, the ruthenium leaching was found to be 2 wt% as confirmed by ICP-MS analysis.
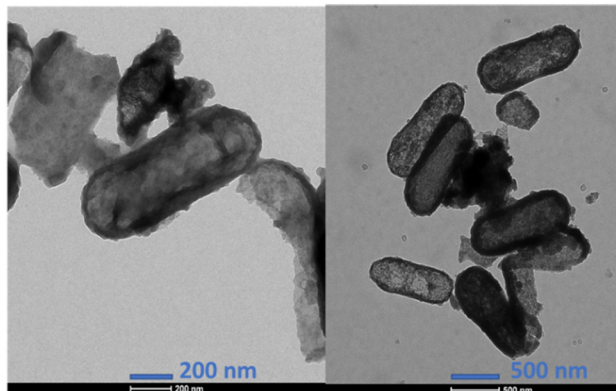
This journal is © The Royal Society of Chemistry 2022

Catal. Sci. Technol., 2022, **12**, 6174–6183 | **6179**

Fig. 7   TEM images of en-HG2@Peanut after 6th run.

with P_2O_5 and distilled under a nitrogen atmosphere prior to use. Hoveyda–Grubbs 2nd generation catalyst (98%) was purchased from ABCR and stored at 2–8 °C under nitrogen atmosphere. The silica gel 60 (70–230 mesh, 480–540 m^2 g^{-1}, pore volume 0.74–0.84 cm^3 g^{-1}) was purchased from Merck and used as received. N_2 physical adsorption tests were performed on a Quantachrome Corporation, Autosorb-6 adsorption analyzer (samples were degassed at 150 °C for 6 h before the measurements). The BET surface areas were evaluated from data in the relative pressure range from 0.05 to 0.25. The total pore volume was estimated from the amount adsorbed at the highest P/P_0 (above 0.99). The surface chemistry of the functionalized particles was analyzed with X-ray photoelectron spectroscopy (XPS) (K-Alpha XPS, ThermoFisher Scientific, U.S.A) in order to characterize the content. Environmental Scanning Electron Microscope (SEM) images were recorded using FEI Quanta 200 FEG ESEM device. Gas chromatography-mass spectrometry (GC-MS) analyses were performed with a Shimadzu GC-MS 2010 Plus using a Restek Rxi-5Sil column (30 m × 0.25 mm × 0.25 μm) and a temperature range of 50–320 °C with a constant helium flow rate of 1 mL min^{-1}. High contrast transmission electron microscopy (TEM) images were recorded at METU Central Lab (Ankara) with FEI Tecnai G2 Spirit Bio(TWIN) 600 TEM at 120 kV using carbon filmed coated copper grids via dropping 1 μL of samples into the grids from EtOH diluted samples.

main reason behind the activity loss was due to the leaching of the catalyst (2 wt% Ru leaching after the 10th run) due to the rupture of the silica shell structure.

To demonstrate the effect of post-pore size reduction in metal leaching, we have recorded the TEM images of non-encapsulated catalyst; HG2@peanut after the first RCM run in DCM. As can be seen in Fig. 8, nano-sized smaller particles were leached from silica gels and cluster-like particles were observed on the outer shell of peanut-shaped silica gels. In addition, in filtrate catalytic tests were carried out to check the ruthenium leaching during RCM reactions. The reaction was initiated with a 2.5 mol% Ru loading in DCM at 30 °C in a Schlenk reactor.

At 60% conversion of diethyl diallylmalonate, the reaction mixture was centrifuged and the samples from upper-liquid phase were taken to another Schlenk reactor. The bottom part of the solution, which is in direct contact with en-HG2@peanut, was taken to a Schlenk reactor and the both reaction mixtures were stirred at 30 °C. As can be seen in Fig. 9, the conversion of diethyl diallylmalonate slightly decreased up to 64% in the absence of the solid catalyst while the reaction mixture containing en-HG2@peanut has reached 99% conversion after one hour. These results showed that the reaction proceeded in a heterogenous manner.

Experimental

Otherwise noted all chemicals were purchased from Sigma-Aldrich and used as received. Dichloromethane was dried
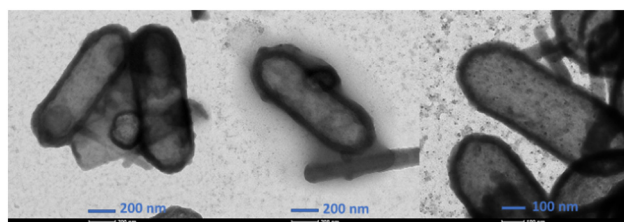
Representative procedure for the synthesis of peanut, capsule and square-shaped hematite colloidal particles

For the synthesis of peanut-shaped hematite colloidal particles, an aqueous solutions of $FeCl_3$ (2 M, 100 mL), Na_2SO_4 (0.6 M, 12 mL), and NaOH (6 M, 90 mL) were added to a 500 mL of glass bottle with a plastic cap at room temperature and stirred under 400 rpm for 15 minutes. Then the bottle was taken to an oven at 100 °C and kept for 8 days. After that, the reaction mixture was taken out of the oven and centrifuged under 6000 rpm for 10 minutes. Then, the Fe_2O_3 particles were washed with DI water and EtOH twice. The particles were first air-dried for 24 h and then dried at 80 °C overnight. Capsule-shaped colloidal particles were synthesized using the same procedure except for the amount of Na_2SO_4 (0.6 M, 10 mL) was decreased. For the square-shaped colloidal particles, the reaction proceeded under similar conditions without Na_2SO_4 addition.[16]

Synthesis of silica-coated hematite colloidal particles

Silica coated hematite particles with different shapes were synthesized based on the Stöber method. Hematite colloidal particles (1.2 g), EtOH (200 mL), DI water (10 mL), Synperonic®F108 (0.2 g), and dodecyltrimethylammonium bromide (CTAB, 0.2 g) were added to a two-necked 500 mL round bottom glass flask, and the reaction mixture was ultrasonicated for 15 minutes. After the ultrasonication, the mixture was stirred with an overhead stirrer at 160 rpm. After
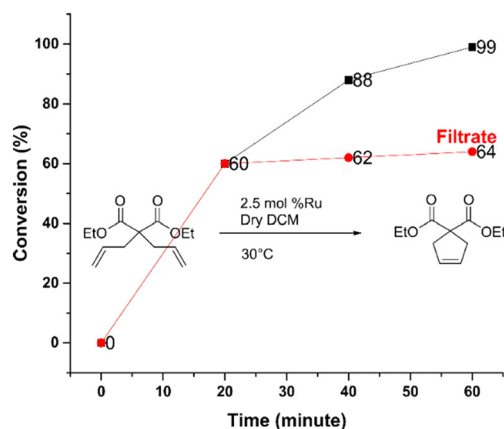

Fig. 8   TEM images of non-encapsulated catalyst (HG2@peanut) after first run.

Fig. 9 In filtrate tests of en-HG2@Peanut in RCM reactions.

30 minutes, the concentrated $NH_3(aq)$ (0.28 M, 2 mL) and TEOS (1 mL) were added dropwise to the flask. The reaction mixture was mechanically stirred for 24 hours. After that, the reaction was stopped and the resulting silica coated particles were separated from the reaction mixture by centrifugation under 6000 rpm for 15 minutes. Next, silica coated particles were washed with DI water and EtOH three times. Then, the particles were dried overnight at 80 °C.

Synthesis of hollow silica gels

Silica-coated hematite colloidal particles (peanut, square, and capsule) were etched with HCl(aq) (6 M) under a reflux system for 24 hours. Then the particles were centrifuged under 6000 rpm for 15 minutes and washed with DI water and EtOH three times. In addition, particles were dried overnight in an oven at 80 °C. Finally, hollow silicas were calcined at 300 °C for 20 hours.

Representative procedure for the preparation of the catalyst

Briefly, the silica gels (30 mg) and dichloromethane (2 mL) were dispersed by ultrasonication for 5 minutes in a 10 mL Schlenk flask. In a different bottle, HG2 (5 mg, 0,080 mmol) catalyst was dissolved in dichloromethane (1 mL) and added to the Schlenk flask and stirred for 12 h under a nitrogen atmosphere. A mild vacuum was applied to remove dichloromethane and then the resulting green powder was washed with dichloromethane (2 mL × 3) and then dried in a vacuum oven overnight. The resulting catalyst was denoted as HG-2@peanut based on the morphology of the silica gel. HG-2@peanut which was obtained from the previous step was taken to a two-necked 100 mL glass flask. The flask was charged with 2 mL dry dichloromethane and then dichlorodiphenyl silane (10 μl, 0.048 mmol, as the pore size reducer) and 2-methylpyridine (0.10 mmol, 10 μl) were added to the flask. The catalyst solution was magnetically stirred at room temperature under $N_2(g)$ for 4 h. After that, dichloromethane was evaporated under a vacuum environment. The resulting catalyst was washed with dichloromethane (1 mL × 2) and dried under a vacuum oven

at 250 C in 70–80 mbar overnight. The encapsulation efficiency was observed as 95% (for peanut) as confirmed by UV-vis analysis. The ruthenium loading was found to be as follows using ICP-MS; 2.17 mmol Ru per g (peanut); 2.05 mmol Ru per g (square), 2.11 mmol Ru per g (capsule).

Representative procedure for ring-closing metathesis reactions

A Sclenk flask was charged with diethyl diallylmalonate (33 μL, 0.133 mmol) and en-HG2@peanut (4 mg, $1.33 × 10^{-3}$ mmol of Ru) in dry dichloromethane (1 mL) under nitrogen atmosphere. The reaction was stirred under 200 rpm at 30 °C. Reaction products were analyzed on GC-MS along with *n*-tetradecane as an internal standard.

Ethenolysis of methyl oleate

Ethenolysis reaction was carried out in a Schlenk flask using technical grade methyl oleate (70% purity). Dry toluene was used as the solvent. The flask was loaded with dry toluene (3 mL) and methyl oleate (21 μL, 0.0604 mmol). Then the flask bubbled with $C_2H_4(g)$ (1 atm) for 5 minutes. In a different bottle, en-HG2@peanut (5 mg, $2.24 × 10^{-4}$ mmol) was dispersed in dry toluene (1 mL), and the catalyst solution was added to the flask. Finally, the flask bubbled again with C_2H_4 for 20 minutes, and the reaction was stirred under 200 rpm at 80 °C. Reaction products were analyzed with GC-MS.

Ethenolysis of fatty acid methyl Ester mixtures (FAME)

Ethenolysis reaction was carried out in a Schlenk flask using fatty acid methyl ester mixtures (rapeseed oil) in dry toluene as the solvent. The flask was loaded with dry toluene (3 mL) and FAME (40 mg, based on the total mole amount of methyl oleate and methyl linoleate; 0.0604 mmol). Then, the flask was bubbled with $C_2H_4(g)$ (1 atm) for 5 minutes. In a different bottle, en-HG2@peanut (5 mg, $2.24 × 10^{-4}$ mmol) was dispersed in dry toluene (1 mL), and the catalyst solution was added to the flask. Finally, the flask was bubbled again with $C_2H_4(g)$ for 20 minutes, and the reaction was stirred under 200 rpm at 80 °C. Reaction products were analyzed with GC-MS.

Reusability test

A Sclenk flask was charged with diethyl diallylmalonate (33 μL, 0.133 mmol) and en-HG2@peanut (4 mg, $1.33 × 10^{-3}$ mmol Ru) in dry dichloromethane (1 mL) under an atmosphere of nitrogen. The reaction was stirred under 200 rpm at 30 °C. Reaction products were analyzed with GC-MS using *n*-tetradecane as an internal standard. When the conversion of diethyl diallylmalonate reached a plateau, the reaction mixture was taken to a falcon tube and centrifuged at 5000 rpm for 4 minutes under an inert nitrogen atmosphere. The organic phase was taken to another flask, and then, the remaining solid catalyst was dispersed in dichloromethane and used in the RCM reactions.

Conclusions

The hollow voids in peanut, square, and capsule-shaped gels provided perfect isolation sites for the encapsulation of HG2. The post-pore size reduction of outer silica gel with dichlorodiphenylsilane prevented the ruthenium from leaching during metathesis reactions by entrapping the catalyst in the inner void. The activity of the encapsulated catalysts (en-HG2@peanut, en-HG2@square and en-HG@capsule) showed superior activity in RCM and ethenolysis reactions, surpassing the homogenous HG2 catalyst, as well as HG2 encapsulated in commercial silica gels (en-HG2@comm.). The catalyst showed improved stability in hollow silica gels, maintaining its activity for up to 6 months in a closed-vessel under the air atmosphere.

Conflicts of interest

There are no conflicts to declare.

Acknowledgements

Notes and references

1 M. Schuster and S. Blechert, *Angew. Chem., Int. Ed. Engl.*, 1997, **36**, 2036–2056.

2 O. M. Ogba, N. C. Warner, D. J. O'Leary and R. H. Grubbs, *Chem. Soc. Rev.*, 2018, **47**, 4510–4544.

3 (*a*) H. Clavier, K. Grela, A. Kirschning, M. Mauduit and S. P. Nolan, *Angew. Chem., Int. Ed.*, 2007, **46**, 6786–6801; (*b*) A. Sytniczuk, M. Dąbrowski, Ł. Banach, M. Urban, S. Czarnocka-Śniadała, M. Milewski, A. Kajetanowicz and K. Grela, *J. Am. Chem. Soc.*, 2018, **140**, 8895–8901.

4 (*a*) B. Alcaide, P. Almendros and A. Luna, *Chem. Rev.*, 2009, **109**, 3817–3858; (*b*) C. Deraedt, M. d'Halluin and D. Astruc, *Eur. J. Inorg. Chem.*, 2013, 4881–4908; (*c*) M. R. Becker, R. B. Watson and C. S. Schindler, *Chem. Soc. Rev.*, 2018, **47**, 7867–7881.

5 (*a*) D. P. Allen, M. M. Van Wingerden and R. H. Grubbs, *Org. Lett.*, 2009, **11**, 1261–1264; (*b*) M. Renom-Carrasco, P. Mania,

R. Sayah, L. Veyre, G. Occhipinti, V. R. Jensen and C. Thieuleux, *Mol. Catal.*, 2020, **483**, 110743; (*c*) H. Balcar and J. Cejka, *Catalysts*, 2019, **9**, 743; (*d*) B. Ö. Öztürk, *Microporous Mesoporous Mater.*, 2018, **267**, 249–256; (*e*) B. Ö. Öztürk, B. Sarıaslan, N. P. Bayramgil and S. K. Şehitoğlu, *Appl. Catal., A*, 2014, **483**, 19–24; (*f*) C. Che, W. Li, S. Lin, J. Chen, J. Zheng, J. Wu, Q. Zheng, G. Zhang, Z. Yang and B. Jiang, *Chem. Commun.*, 2009, 5990–5992.

6 X. S. Zhao, X. Y. Bao, W. Guo and F. Y. Lee, *Mater. Today*, 2006, **9**, 32–39.

7 N. End and K. U. Schöning, Immobilized Catalysts in Industrial Research and Application, in *Immobilized Catalysts, Topics in Current Chemistry*, ed. A. Kirschning, Springer, Berlin, Heidelberg, 2004, vol. 242.

8 (*a*) B. Ö. Öztürk, B. Durmuş and S. Karabulut Şehitoğlu, *Catal. Sci. Technol.*, 2018, **8**, 5807–5815; (*b*) D. Astruc, A. K. Diallo, S. Gatard, L. Liang, C. Ornelas, V. Martinez and D. Méry, *Beilstein J. Org. Chem.*, 2011, **7**, 94–103; (*c*) M. Zarka, O. Nuyken and R. Weberskirch, *Macromol. Rapid Commun.*, 2004, **25**, 858–862.

9 (*a*) S. Zhang, B. Zhang, H. Liang, Y. Liu, Y. Qiao and Y. Qin, *Angew. Chem., Int. Ed.*, 2018, **57**, 1091–1095; (*b*) S. A. Dergunov, A. T. Khabiyev, S. N. Shmakov, M. D. Kim, N. Ehterami, M. C. Weiss, V. B. Birman and E. Pinkhassik, *ACS Nano*, 2016, **10**, 11397–11406; (*c*) L. J. Jongkind, M. Rahimi, D. Poole III, S. J. Ton, D. E. Fogg and J. N. H. Reek, *ChemCatChem*, 2020, **12**, 4019–4023; (*d*) Y. Shen, Z. F. Li, S. Y. Guo, Y. R. Shao and T. L. Hu, *ACS Appl. Mater. Interfaces*, 2021, **13**, 12169–12180; (*e*) B. Ö. Öztürk, B. Çetinel and S. Karabulut Şehitoğlu, *Appl. Organomet. Chem.*, 2020, **34**, 5686; (*f*) D. Wang, S. Li, C. Wu and T. Li, *J. Am. Chem. Soc.*, 2022, **144**, 685–689; (*g*) G. Pareras, D. Tiana and A. Poater, *Catalysts*, 2020, **10**, 687; D. Wang, S. Li, C. Wu and T. Li, *J. Am. Chem. Soc.*, 2022, **144**, 685–689.

10 (*a*) H. Yang, L. Zhang, L. Zhong, Q. Yang and C. Li, *Angew. Chem., Int. Ed.*, 2007, **46**, 6861–6865; (*b*) H. Q. Yang, L. Zhang, P. Wang, Q. H. Yang and C. Li, *Green Chem.*, 2009, **11**, 257–264; (*c*) R. L. Oliveira, T. Nijholt, M. Shakeri, P. E. de Jongh, R. J. M. K. Gebbink and K. P. de Jong, *Catal. Sci. Technol.*, 2016, **6**, 5124–5133; (*d*) G. Purohit, D. S. Rawat and O. Reiser, *ChemCatChem*, 2020, **12**, 569–575.

11 H. Yang, Z. Ma, T. Zhou, W. Zhang, J. Chao and Y. Qin, *ChemCatChem*, 2013, **5**, 2278–2287.

12 Q. Li, T. Zhou and H. Yang, *ACS Catal.*, 2015, **5**, 2225–2231.

13 Z. Tunalı, K. Sagdic, F. Inci and B. Ö. Öztürk, *React. Chem. Eng.*, 2022, **7**, 1617–1625.

14 J. Sharma and G. Polizos, *Nanomaterials*, 2020, **10**, 1599.

15 (*a*) J. C. Song, F. F. Xue, Z. Y. Lu and Z. Y. Sun, *Chem. Commun.*, 2015, **51**, 10517; (*b*) H. Yang and Z. Xin, *Langmuir*, 2018, **34**, 11723–11728.

16 Y. Wang, X. Su, P. Ding, S. Lu and H. Yu, *Langmuir*, 2013, **29**, 11575–11581.

17 C. Gao, F. Lyu and Y. Yin, *Chem. Rev.*, 2021, **121**, 834–881.

18 Y. Bao, T. Wang, Q. Kang, C. Shi and J. Ma, *Sci. Rep.*, 2017, **7**, 46638.

19 (*a*) K. S. W. Sing, *Pure Appl. Chem.*, 1982, **54**, 2201–2218; (*b*) H. Yang, Z. Ma, Y. Wang, Y. Wang and L. Fang, *Chem. Commun.*, 2010, **46**, 8659–8661.

20 (*a*) J. Bidange, C. Fischmeister and C. Bruneau, *Chem. – Eur. J.*, 2016, **22**, 12226–12244; (*b*) U. Biermann, U. Bornscheuer, M. A. R. Meier, J. O. Metzger and H. J. Schäfer, *Angew. Chem., Int. Ed.*, 2011, **50**, 3854–3871; (*c*) H. Mutlu, R. Hofsäß, R. E. Montenegro and M. A. R. Meier, *RSC Adv.*, 2013, **3**, 4927–4934.

21 (*a*) G. A. Bailey, M. Foscato, C. S. Higman, C. S. Day, V. R. Jensen and D. E. Fogg, *J. Am. Chem. Soc.*, 2018, **140**, 6931–6944; (*b*) P. D. Nieres, J. Zelin, A. F. Trasarti and C. R. Apesteguía, *Catal. Sci. Technol.*, 2016, **6**, 6561–6568; (*c*) S. C. Marinescu, R. R. Schrock, P. Müller and A. H. Hoveyda, *J. Am. Chem. Soc.*, 2009, **131**, 10840–10841; (*d*) J. Zhang, S. Song, X. Wang, J. Jiao and M. Shi, *Chem. Commun.*, 2013, **49**, 9491–9493.

22 B. Ö. Öztürk, B. Topoğlu and S. Karabulut Şehitoğlu, *Eur. J. Lipid Sci. Technol.*, 2015, **117**, 200–208.

23 Z. Al-Hamamre, S. Foerster, F. Hartmann, M. Kröger and K. Martin, *Fuel*, 2012, **96**, 70–76.

24 (*a*) J. Morvan, M. Mauduit, G. Bertrand and R. Jazzar, *ACS Catal.*, 2021, **11**, 1714–1748; (*b*) A. Kajetanowicz, M. Chwalba, A. Gawin, A. Tracz and K. Grela, *Eur. J. Lipid Sci. Technol.*, 2020, **122**, 1900263.